PNAS RESEARCH ARTICLE | MEDICAL SCIENCES

Tumor progression is independent of tumor-associated macrophages in cell lineage–based mouse models of glioblastoma

Mollie E. Chipman[a,b,c], Zilai Wang[a,b,1], Daochun Sun[a,b,2], Alicia M. Pedraza[a], Tejus A. Bale[a,d], and Luis F. Parada[a,b,3]

Contributed by Luis F. Parada; received January 6, 2023; accepted March 9, 2023; reviewed by Dolores Hambardzumyan and Russell Pieper

Macrophage targeting therapies have had limited clinical success in glioblastoma (GBM). Further understanding the GBM immune microenvironment is critical for refining immunotherapeutic approaches. Here, we use genetically engineered mouse models and orthotopic transplantation-based GBM models with identical driver mutations and unique cells of origin to examine the role of tumor cell lineage in shaping the immune microenvironment and response to tumor-associated macrophage (TAM) depletion therapy. We show that oligodendrocyte progenitor cell lineage-associated GBMs (Type 2) recruit more immune infiltrates and specifically monocyte-derived macrophages than subventricular zone neural stem cell-associated GBMs (Type 1). We then devise a TAM depletion system that offers a uniquely robust and sustained TAM depletion. We find that extensive TAM depletion in these cell lineage–based GBM models affords no survival benefit. Despite the lack of survival benefit of TAM depletion, we show that Type 1 and Type 2 GBMs have unique molecular responses to TAM depletion. In sum, we demonstrate that GBM cell lineage influences TAM ontogeny and abundance and molecular response to TAM depletion.

glioblastoma | tumor-associated macrophages | cell of origin | CSF1R inhibition | microglia

Glioblastoma (GBM) is an aggressive primary brain tumor with a dismal five-year survival rate of five percent (1). Standard of care therapy is surgery followed by radiation and chemotherapy with tumor-treating fields (2). Given that TAMs can constitute up to forty percent of live cells in GBM, it's logical to examine their functions in tumor development and progression to assess their value as possible therapeutic targets (3).

In GBM, TAMs are composed of both tissue-resident microglia and monocyte-derived macrophages (MDMs) infiltrating from the periphery (4). TAMs have primarily been reported to exhibit protumorigenic functions, including promoting angiogenesis, secreting tumor-supportive growth factors, and suppressing antitumor immunity (5–8). However, recent single-cell RNA sequencing studies have highlighted the heterogeneity of TAM populations in GBM (9–11) and have shown that some TAM populations support antitumor immunity (12), while some populations support tumor growth (5). Overall, the role of TAMs in GBM is complex (13) and incompletely understood.

Because TAMs rely on CSF1-CSF1R signaling for proliferation and survival, several studies have tested the effect of CSF1R inhibition on GBM survival. Targeting TAMs with CSF1R inhibitor was reported as highly effective in RCAS PDGFB-driven models of GBM (14, 15). However, despite promising preclinical studies, CSF1R inhibitor therapy did not show population-wide success in GBM clinical trials (16). In this clinical trial (16), two patients showed an extended progression-free survival, suggesting that subsets of GBM may indeed respond to CSF1R therapy. More recently, CSF1R inhibitor therapy was tested in several mouse models of GBM with differing driver mutations; success was again seen in PDGFB-driven GBM, but not in H-Ras or PDGFRA-driven models (17). These studies highlight the diversity of models and that a more basic understanding of the GBM tumor immune microenvironment as well as more cohesive preclinical data are needed.

Here, we explore how GBM cell lineage association influences the tumor immune microenvironment composition and response to TAM depletion using mouse models harboring identical and physiologically relevant driver mutations (*Nf1*, *Trp53*, and *Pten*) with unique cells of origin (18). We show that while both tumor types exhibit immune infiltration, oligodendrocyte progenitor cell (OPC) lineage-derived GBMs recruit significantly greater numbers of MDMs compared to subventricular zone (SVZ) neural stem cell (NSC)-derived GBMs. To examine the role of TAMs in tumor development and progression, we combine a genetic and pharmacologic approach to achieve effective and sustained TAM depletion beyond the effects of CSF1R inhibitor therapy alone. Acute

Significance

Further understanding the glioblastoma (GBM) tumor immune microenvironment to refine immunotherapeutic strategies is essential. Here, we show that GBM tumor cell lineage association can influence the abundance and ontogeny of tumor-associated macrophages (TAMs) in the tumor immune microenvironment. Despite differential immune microenvironment composition, TAM depletion results in no survival extension in all models tested. Although TAM depletion does not extend survival, we show that subventricular zone neural stem cell-associated GBMs (Type 1) and oligodendrocyte progenitor cell lineage-associated GBMs (Type 2) have unique transcriptional responses to TAM depletion. We highlight that although TAMs provide important tumor-supportive signals, some GBMs do not depend on them for survival.

Reviewers: D.H., Icahn School of Medicine at Mount Sinai Department of Medicine; and R.P., University of California San Francisco.

The authors declare no competing interest.

[1]Present address: Chicago BioSolutions Inc., Chicago, IL 60612.

[2]Present address: Department of Cell Biology, Neurobiology, and Anatomy, Medical College of Wisconsin, Wauwatosa, WI 53226.

[3]To whom correspondence may be addressed. Email: paradal@mskcc.org.

This article contains supporting information online at https://www.pnas.org/lookup/suppl/doi:10.1073/pnas.2222084120/-/DCSupplemental.

Published April 11, 2023.

and chronic TAM depletion in our lineage-based models of GBM showed no significant modulation of tumor initiation, progression, or survival extension.

Results

Cell of Origin Impacts Immune Microenvironment. To investigate the impact of cell of origin on the tumor immune microenvironment in GBM, we used two experimental systems: spontaneous genetic models and allograft models. In the spontaneous model, tumor suppressor loss is induced in the adult SVZ by tamoxifen induction of *Nst-CreER^{T2}; Nf1$^{fl/+}$; Trp53$^{fl/fl}$; Pten$^{fl/+}$* mice to form Type 1 GBM (19). Alternatively, tumor suppressor recombination is induced in progenitor cells of the oligodendrocytic lineage by tamoxifen induction of *NG2-CreER^{TM}; Nf1$^{fl/+}$; Trp53$^{fl/fl}$; Pten$^{fl/+}$* mice to form Type 2 GBM (19) (Fig. 1*A*). Primary cultures from the Type 1 and Type 2 spontaneous tumors can be grown in a defined serum-free medium and orthotopically injected into immunocompetent mice (19) (*SI Appendix*, Fig. S1*A*). These models have been extensively characterized (18) and offer a physiologically relevant and immunocompetent system to study the tumor immune microenvironment.

TAM morphology and quantity were assessed in the spontaneous tumor cores using immunohistochemical staining with IBA1 antibody. Type 1 (SVZ NSC lineage) tumors exhibited fewer TAMs albeit with a greater number of processes than Type 2 (oligodendrocyte lineage) GBM TAMs (Fig. 1 *B* and *C*). MDMs are known to have fewer processes compared to resident microglia (20), thus suggesting that Type 2 GBMs have greater MDM infiltration. We also examined the TAM composition in orthotopically transplanted tumors and found similar results as the spontaneous tumors with greater number of TAMs in the oligodendrocyte lineage-associated (Type 2) tumors (*SI Appendix*, Fig. S1*B*). To assess the ontogeny and spatial distribution of TAMs in spontaneous Type 1 and Type 2 GBMs, CD44, a marker of MDMs (9), was used in conjunction with IBA1. We observed a significant increase in IBA1+, CD44+ cells in the tumor core and IBA1, CD44- cells in the parenchyma of Type 2 GBMs, consistent with our observations on the morphology difference of Type 1 and Type 2 GBM TAMs (*SI Appendix*, Fig. S1*C*). Overall, the majority of MDMs are in the tumor cores of Type 1 and Type 2 GBMs, while microglia are present in the tumor core, border, and brain parenchyma, likely reflecting preferential tumor entry zones with MDMs entering via neoangiogenic vessels (*SI Appendix*, Fig. S1*C*). To assess TAM ontogeny and spatial distribution in Type 1 and Type 2 transplanted GBMs, lineage tracing was employed using

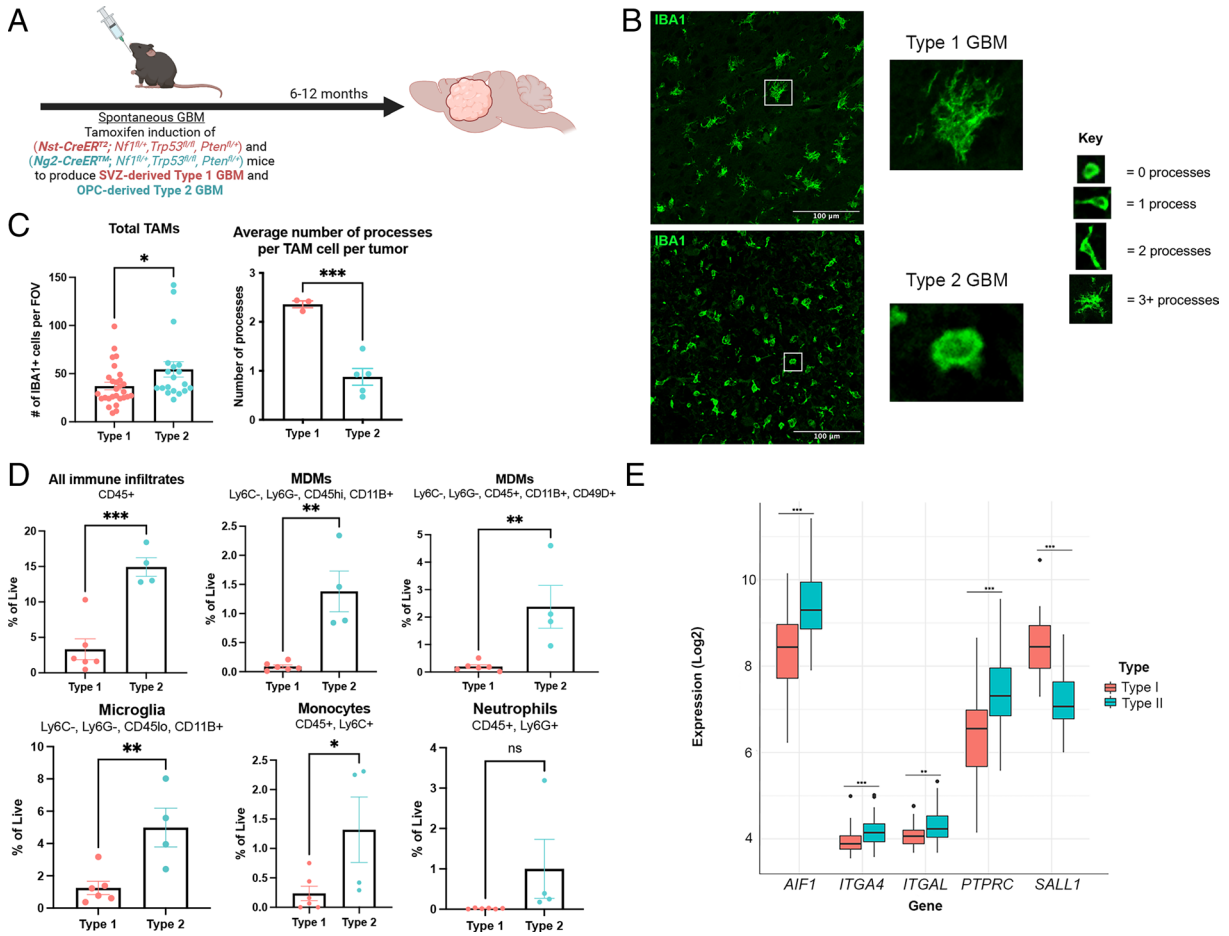

Fig. 1. Cell of origin influences TAM ontogeny in spontaneous GEMMs of GBM. (*A*) Schematic illustrating the spontaneous GEMMs used to examine the impact of GBM cell of origin on the tumor immune microenvironment. (*B* and *C*) IF images and quantification of the total TAMs in Type 1 and Type 2 spontaneous GBMs (N = 6 Type 1, 4 Type 2 tumors, data represented as mean with SEM, $P = 0.0379$, unpaired t test, each dot represents one FOV) and the average number of processes per TAM cell per tumor (N = 3 Type 1, 5 Type 2, TAMs quantified from five 20× images per tumor, data represented as mean with SEM, $P = 0.0007$, unpaired t test). (*D*) Multicolor flow cytometry measuring the levels of all immune infiltrates ($P = 0.0006$), MDMs ($P = 0.0017$ CD45^{hi}, CD11B^{+}, $P = 0.0082$ CD45^{+}, CD11B^{+}, CD49D^{+}), microglia ($P = 0.0086$), neutrophils, and monocytes ($P = 0.0489$), data represented as mean with SEM, unpaired t test, each dot represents one mouse. (*E*) mRNA expression levels of pan-TAM (AIF1), MDM-associated (ITGA4, ITGAL), pan-immune (PTPRC), and microglia-associated (SALL1) genes in Type 1 and Type 2 subtyped human TCGA GBM samples (N = 52 core Type I, 38 core Type II).

Cx3cr1-CreER^{T2}-Ires-Yfp; Lsl-Tdt mice. Microglia retain Tdt positivity over time and were quantified as Tdt+, IBA1+ cells, while MDMs lose Tdt positivity over time, and were thus quantified as Tdt-, IBA1+ cells. Again, Type 2 GBMs had significantly greater amounts of IBA1+, Tdt- MDMs in the tumor core (*SI Appendix*, Fig. S1*D*). The spatial distribution of TAMs mirrored that seen in spontaneous GBMs, as the majority of MDMs are localized to the tumor core, while microglia are distributed throughout the tumor core, border, and brain parenchyma (*SI Appendix*, Fig. S1*D*).

To further characterize the microenvironments of spontaneous Type 1 and Type 2 GBM, multicolor flow cytometry was used to quantify myeloid and lymphoid populations (*SI Appendix*, Fig. S2*A*). Type 2 GBM showed significantly higher levels of CD45+ immune infiltrates, characterized by increased levels of MDMs, microglia, monocytes, and neutrophils (Fig. 1*D*). Increased levels of MDMs were verified using an independent MDM marker, CD49D (21) (Fig. 1*D*). In contrast, relative lymphoid cell levels were not significantly different between Type 1 and Type 2 tumors, aside from a nonsignificant increase in CD4+ T cells in Type 2 tumors (*SI Appendix*, Fig. S2*B*). We next examined transplanted tumors and found similar immune microenvironment composition with Type 2 tumors exhibiting significantly higher levels of total immune infiltrate, MDMs, and neutrophils and trending higher levels of monocytes and microglia (*SI Appendix*, Fig. S1*E*). No change in lymphocyte populations was observed (*SI Appendix*, Fig. S1*E*). Again, increased levels of MDMs were verified with the independent MDM marker, CD49D (21) (*SI Appendix*, Fig. S1*E*). We note that although the TAM trends in spontaneous tumors are mirrored in transplanted tumors, we do see a higher recruitment of MDMs and almost all peripherally derived immune cell types in transplanted tumors, as reported elsewhere (22). This is likely due to the higher growth rate of transplanted tumors (~6 to 8 wk for transplanted tumors compared to ~6 to 12 mo for spontaneous tumors) and the potential inflammation induced by transplantation surgery. In aggregate, these data indicate that in the context of identical driver mutations, cell of origin and lineage influence the microenvironment composition wherein Type 2 GBMs recruit more TAMs, and particularly MDMs, than Type 1 tumors.

Having previously identified cohorts of Type 1 and Type 2 GBM in the TCGA human GBM data repository, termed Type I and Type II GBM to denote human tumors, we probed these datasets for expression of TAM-associated genes (18, 23, 24). We found, consistent with the mouse modeling data, that expression of the pan-TAM marker gene *AIF1*, pan-immune infiltrate marker *PTPRC*, and MDM marker genes, *ITGA4* and *ITGAL* (21), were significantly higher in human Type II tumor data (Fig. 1*E*). This suggests that human Type II GBMs have more total immune infiltration and MDMs than human Type I GBMs. Additionally, *SALL1*, a microglial marker gene (25), was significantly higher in Type I human tumors (Fig. 1*E*). Overall, these analyses demonstrate that oligodendrocyte lineage-associated GBMs contain substantially greater MDM numbers in both mouse Type 2 and human Type II GBM.

Transcriptional TAM Cohesion in Transplanted and Spontaneous GBM. To determine the transcriptional states of TAMs in spontaneous and transplanted GBM, we performed bulk RNA-sequencing on sorted MDMs (Ly6C$^-$, Ly6G$^-$, CD45^{hi}, and CD11B$^+$) and microglia (Ly6C$^-$, Ly6G$^-$, CD45^{lo}, and CD11B$^+$). Tumors were dissociated on ice prior to sorting to avoid acute transcriptome modifications (*SI Appendix*, Fig. S3*A*) (26). Samples underwent principal component analysis and the data revealed that the most significant driver of TAM transcriptional grouping was ontogeny (MDM vs. Microglia) and not whether the tumors arose spontaneously or were subjected to allograft transplantation (3, 21) (*SI Appendix*, Fig. S3*B*). Consequently, levels of genes known to mark MDMs (*Itga4, Cd44, and Itgal*) (9, 21) and microglia (*Tmem119, Sall1, Cx3cr1, and P2ry12*) (25, 27) were elevated in their respective samples (*SI Appendix*, Fig. S3*C*). We noted 4,199 differentially expressed genes between all MDM vs. all microglia samples (Padj < 0.05, LFC > 1.5 or LFC < −1.5), with 1,728 enriched in microglia and 2,471 enriched in MDMs (*SI Appendix*, Fig. S3*D*, and Dataset S1). Genes enriched in microglia were associated with gene ontology terms for neurological processes and angiogenesis, while genes enriched in MDMs were associated with cell adhesion, antigen presentation, and lymphocyte activation, consistent with previous reports (3, 28)(*SI Appendix*, Fig. S3 *E* and *F*). We also examined the influence of cell of origin on TAM transcriptome and found no appreciable differences; TAM populations did not group by the tumor type they were derived from on the PCA plot. Overall, because TAMs in spontaneous and orthotopically transplanted GBMs are transcriptionally similar, we moved forward with the orthotopic transplantation model to examine the role of TAMs in tumor progression.

A Robust TAM Depletion System. To investigate the potential role of TAMs in GBM development, we evaluated different strategies for effective TAM depletion. We first employed a TAM-specific promoter *Cx3cr1-CreER^{T2}-Ires-Eyfp* transgene to drive homologous recombination (29) of a Cre-dependent diphtheria toxin receptor (*R26-Lsl-iDTR*) and Td-Tomato reporter (*R26-Lsl-Tdt*) cassettes thus permitting TAM visualization and rendering them diphtheria toxin (DT) sensitive. Tamoxifen dosing was optimized for high iDTR recombination efficiency and approximately 90 to 95% recombination was achieved with two doses given 24 h apart (*SI Appendix*, Fig. S4 *A* and *B*). We next treated nontumor-bearing mice with three initial DT doses, 24 h apart, and continued dosing every three days thereafter for 2 wk to maintain microglia depletion. Microglia depletion was effective for up to 72 h after the initial DT doses; however, the maintenance regimen was unsuccessful as we observed rapid repopulation by DTR nonexpressing microglia (*SI Appendix*, Fig. S4*C*). This effect of rapid microglia repopulation was likely due to Cre recombination inefficiency that allowed a few remaining iDTR- microglia to mediate reconstitution. To improve the maintenance of microglia depletion, the mice were placed on CSF1R inhibitor (PLX5622; CSF1Ri) containing chow following the initial three doses of DT (*SI Appendix*, Fig. S4*D*). This combined targeting approach resulted in robust, sustained microglia depletion in normal brains (87% cortex depletion after 1 wk of treatment, 86% after 2 wk of treatment) and worked better than CSF1R inhibition alone, particularly in the first week of treatment (66% cortex depletion after 1 wk, 81% cortex depletion after 2 wk) (Fig. 2 *A* and *B*). The combined depletion strategy in Type 1 and Type 2 GBMs also achieved significant depletion (~84% in Type 1, ~97% in Type 2) of total TAMs and depletion of monocytes, with no evident changes in neutrophil levels or significant impact on the lymphoid compartment (Fig. 2*C* and *SI Appendix*, Fig. S4*E*). In sum, our TAM depletion system has greater efficacy and sustainability than previously reported strategies (9, 14, 17, 30).

TAM Depletion Does Not Extend Survival. Following TAM depletion in Type 1 and Type 2 GBMs, we examined tumor progression (*SI Appendix*, Fig. S4*D*). In the first set of experiments, TAM depletion was initiated approximately 3 to 4 wk after tumor

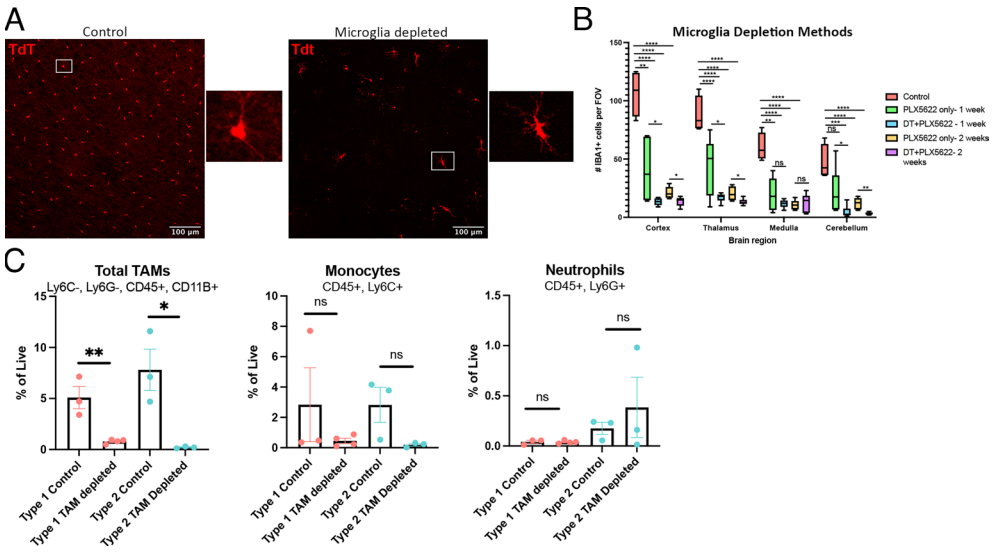

Fig. 2. Combination of a genetic and pharmacologic system robustly depletes TAMs. (*A*) Representative IF images of microglia-depleted vs. control nontumor bearing brains. (*B*) Box and whisker plot comparing microglia depletion strategies. N = 2 mice per group, three images quantified per mouse per brain region, middle line displays median value, whiskers display min and max values. Comparing the median values for the cortex region gives the following TAM depletion percentages by treatment; 66% (CSF1R only 1 wk), 81% (CSF1R only 2 wk), 87% (DT+CSF1R 1 wk), 86% (DT+CSF1R 2 wk). All *P* values with four stars indicate $P < 0.0001$. Other *P* values for comparisons are cortex 1 wk DT+PLX5622 vs. PLX5622 only ($P = 0.041$), cortex 2 wk DT+PLX5622 vs. PLX5622 only ($P = 0.016$), thalamus 1 wk DT+PLX5622 vs. PLX5622 only ($P = 0.023$), thalamus 2 wk DT+PLX5622 vs. PLX5622 only ($P = 0.019$), cerebellum 1 wk DT+PLX5622 vs. PLX5622 only ($P = 0.05$), cerebellum 2 wk DT+PLX5622 vs. PLX5622 only ($P = 0.0015$), cortex 1 wk control vs. PLX5622 only ($P = 0.0037$), medulla 1 wk control vs. PLX5622 only ($P = 0.0014$), and cerebellum 1 wk control vs. DT+PLX5622 ($P = 0.0002$). (*C*) Multicolor flow cytometry levels of total TAMs (Type 1 $P = 0.0056$, Type 2 $P = 0.02$), monocytes, and neutrophils in control vs. TAM-depleted Type 1 and Type 2 GBMs, data represented as mean with SEM, unpaired *t* test, each dot represents one mouse. TAM depletion percentage was estimated by comparing the percentages of total TAMs between TAM-depleted and control samples (84% for Type 1, 97% for Type 2).

implantation allowing for GBM establishment. We observed no effects, either acceleration or delay, in survival of either Type 1 or Type 2 GBM models (Fig. 3 *A* and *B*). Additionally, TAM depletion did not impact tumor cell proliferation, as measured by phospho-histone H3 (PH3) and Ki67 staining (Fig. 3*C*, and *SI Appendix*, Fig. S5*A*), or tumor histology (*SI Appendix*, Fig. S5 *B* and *C*). To examine the impact of TAM depletion on the early stages of tumor initiation, TAM depletion was implemented in Type 2 tumors 1 wk after tumor implantation. This protocol also failed to modify tumor-bearing mouse survival (Fig. 3*D*). These results are consistent with recent reports that Ras-driven GBMs do not respond to TAM depletion therapy (17).

We also employed our TAM depletion strategy on a Ras-independent GBM model using a primary tumor line generated from a spontaneous GBM mouse with the genetic configuration: *Nst-CreER*^{T2}*; Qk*$^{fl/fl}$*; Trp53*$^{fl/fl}$*; Pten*$^{fl/fl}$ (22, 31). TAM depletion was also unsuccessful in extending mouse survival in *Nf1* sufficient GBM (Fig. 3*E*). Taken together, our data indicate that in a setting where we maximally deplete TAMs, either early in tumor initiation or during progression, tumor development remains unimpeded.

Type 1 and Type 2 GBMs Have Distinct Molecular Responses to TAM Depletion. To understand how TAM depletion impacted the GBM transcriptome, we performed bulk RNA sequencing of Type 1 and Type 2 TAM-depleted vs. control GBM bulk tumor tissue. All samples were analyzed by principal component analysis and as illustrated by PCA plot, Type 1 and Type 2 GBMs still group separately on the plot, regardless of the TAM depletion status (*SI Appendix*, Fig. S6*A*). We found 1,185 differentially expressed genes between all TAM-depleted vs. control GBMs (Padj < 0.05, LFC >1.5 or LFC < −1.5). Further, 272 genes were enriched in TAM-depleted GBM transcriptomes, while the remaining 913 DEGs were decreased (*SI Appendix*, Fig. S6*B* and Dataset S2). The genes with decreased expression were primarily immune related, consistent with depletion of TAMs, and pathways such as Hallmark Interferon Alpha Response and Hallmark Interferon Gamma Response were significantly reduced (*SI Appendix*, Fig. S6 *C*–*E*, and Dataset S2). Examining the transcriptionally increased genes revealed the enrichment of pathways related to tumor growth, such as Hallmark Hedgehog signaling and Hallmark Mitotic Spindle, consistent with previous reports (17) (*SI Appendix*, Fig. S6 *D* and *F*).

Next, we analyzed the Type 1 and Type 2 samples separately for their transcriptional response to TAM depletion. When analyzed independently, TAM-depleted samples separated from control samples in both Type 1 and Type 2 GBMs (Fig. 4 *A* and *B*). Of note, 192 genes were enriched and 3756 genes decreased in Type 1 TAM-depleted GBMs, and 843 genes were enriched and 311 genes decreased in Type 2 TAM-depleted GBMs (Padj < 0.05, LFC >1.5 or LFC < −1.5) (Fig. 4 *C* and *D* and Dataset S2). We performed GSEA and found that Type 1 GBMs up-regulated more progrowth-related pathways than Type 2 GBMs, while Type 2 GBMs only significantly up-regulated hallmark oxidative phosphorylation (Fig. 4 *E* and *F*). Type 2 GBMs had more immune related hallmark pathways significantly decreased compared to Type 1 GBMs, consistent with Type 2 GBMs having a greater immune component than Type 1 GBMs (Fig. 4 *E* and *F*). Overall, this analysis suggests that while there was no survival benefit afforded to either Type 1 or Type 2 TAM-depleted GBMs, Type 1 and Type 2 GBMs responded differently to TAM depletion on the molecular level.

Discussion

Macrophage-targeted therapies have thus far been unsuccessful in cancer (32). However, many clinical trials are ongoing assessing the potential clinical benefit of depleting TAMs, reprograming TAMs toward a proinflammatory phenotype, bolstering phagocytosis, altering TAM recruitment, and engineering macrophages to deliver cytokines to the TIME or selectively kill cancer cells (32). Given

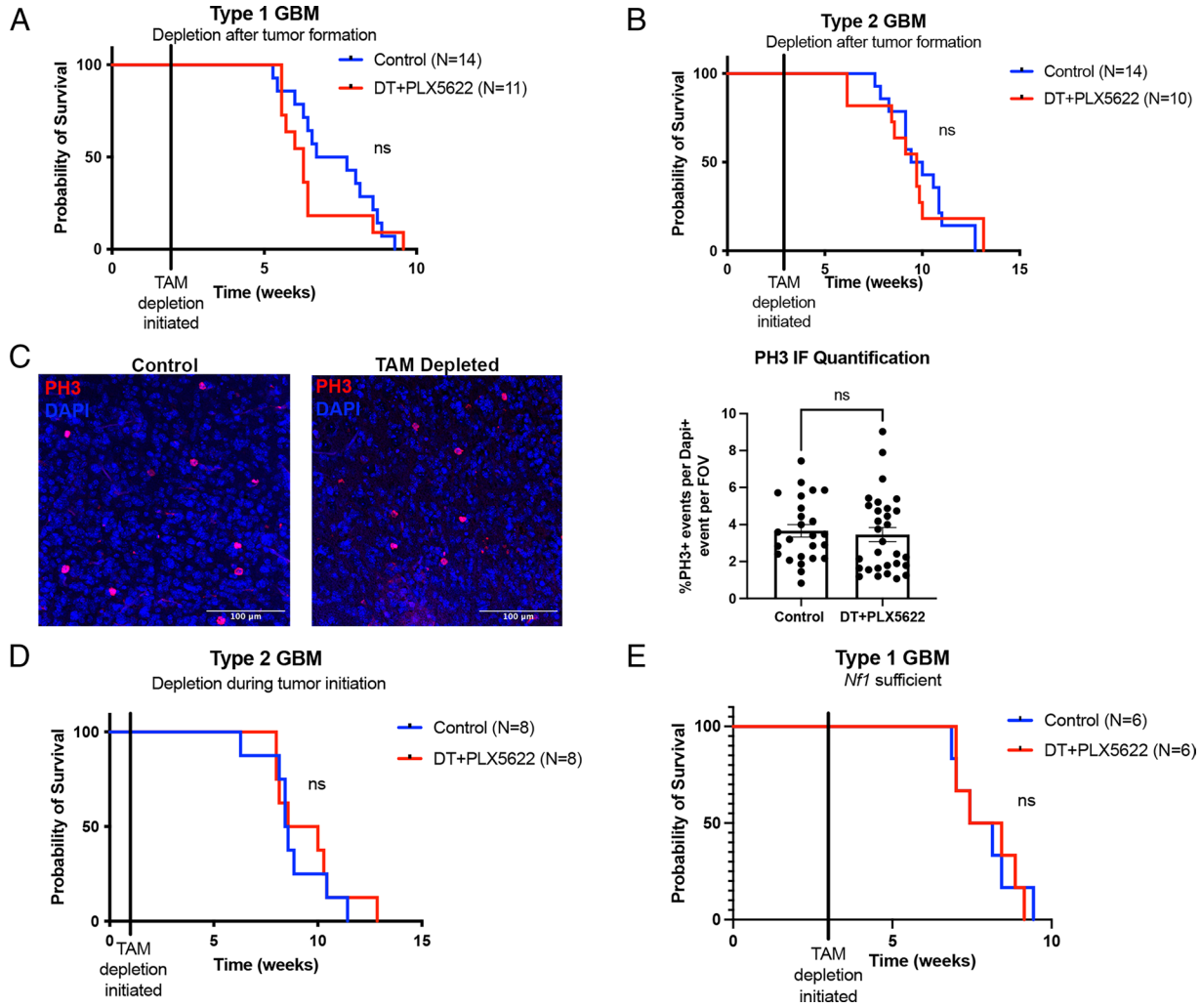

Fig. 3. TAM depletion does not extend survival in Type 1 and Type 2 GBM. Kaplan–Meier survival curves of TAM-depleted vs. control (treatments initiated 3 to 4 wk after tumor implantation) Type 1 (DT+PLX5622 N = 11, Control N = 14, median survival of 7.2 wk for control, 6.3 wk for DT+PLX5622) (*A*) and Type 2 (DT+PLX5622 N = 10, Control N = 14, median survival of 9.7 wk for control, 9.7 wk for DT+PLX622) (*B*) GBM mice, significance calculated with Mantel–Cox test. (*C*) Phospho-histone H3 IF staining images and quantification of TAM-depleted and control GBMs, data represented as mean with SEM, N= 5 control mice, 5 TAM-depleted mice, unpaired *t* test, symbols represent %PH3+ events per dapi+ event for each FOV (5 FOV per mouse). (*D*) Kaplan–Meier survival curve of TAM-depleted vs. control (treatments initiated 1 wk after tumor implantation) Type 2 (DT+PLX5622 N = 8, control N = 8, median survival of 8.5 wk for control, 9.3 wk for DT+PLX622) GBM mice, significance calculated with the Mantel–Cox test. (*E*) Kaplan–Meier survival curve of TAM-depleted vs. control (initiated 3 to 4 wk after tumor implantation) *Nf1*-sufficient (DT+PLX5622 N = 6, Control N = 6, median survival of 7.8 wk for control, 7.9 wk for DT+PLX5622) GBM mice, significance calculated with the Mantel–Cox test.

the high abundance of TAMs in GBMs, examining the potential of TAM-targeted therapies in GBM is imperative. Preclinical studies have shown benefit in inhibiting CSF1R signaling (9, 14, 15), decreasing recruitment of TAMs with LOX inhibition (8), combining CD47 blockade with temozolomide (33) or radiation and fatty acid oxidation inhibitors (34), and engineering Tie-2 expressing monocytes to deliver IFN-alpha to the TIME (35), among other approaches.

Although initial studies targeting TAM proliferation and survival with CSF1R inhibitors showed significant survival extension in mouse models of GBM (14, 15), population-wide efficacy was not seen in a Phase I/II clinical trial in recurrent GBM (16). More recent reports testing CSF1R inhibitors in mouse models of GBM have seen mixed results, with the treatment extending survival in some mouse models and hindering or not impacting survival in others (9, 17). Thus, more cohesive preclinical data as well as potential biomarkers of response to CSF1R inhibition are needed.

Here, we investigated GBM cell of origin (or transcriptional lineage association) as a potential stratification for TAM-targeted therapies. GEMMs that developed spontaneous GBM by initiation in SVZ stem cells or oligodendrocytic progenitor cells gave rise to GBM with distinguishable molecular and histological features (18). We found that these distinguishing features extend beyond tumor cells to the tumor immune microenvironment. We identified marked differences in TAM ontogeny, with oligodendrocytic-derived Type 2 GBM exhibiting substantially greater recruitment of peripherally derived MDMs, while Type 1 GBM primarily recruited resident microglia. We further extended these findings from spontaneous GEMMs to orthotopic transplantation models and finally in human patients using the Type I and Type II subtyped samples in the TCGA dataset (18). These results could have implications for TAM targeting approaches which may have more favorable outcomes if confined to the more MDM-rich Type II tumors.

As an additional approach to validate the relevance of studying TAMs in orthotopic transplantation models of GBM, we performed sorted RNA-sequencing on Type 1 and Type 2 GBM-derived microglia and MDMs. The results demonstrated

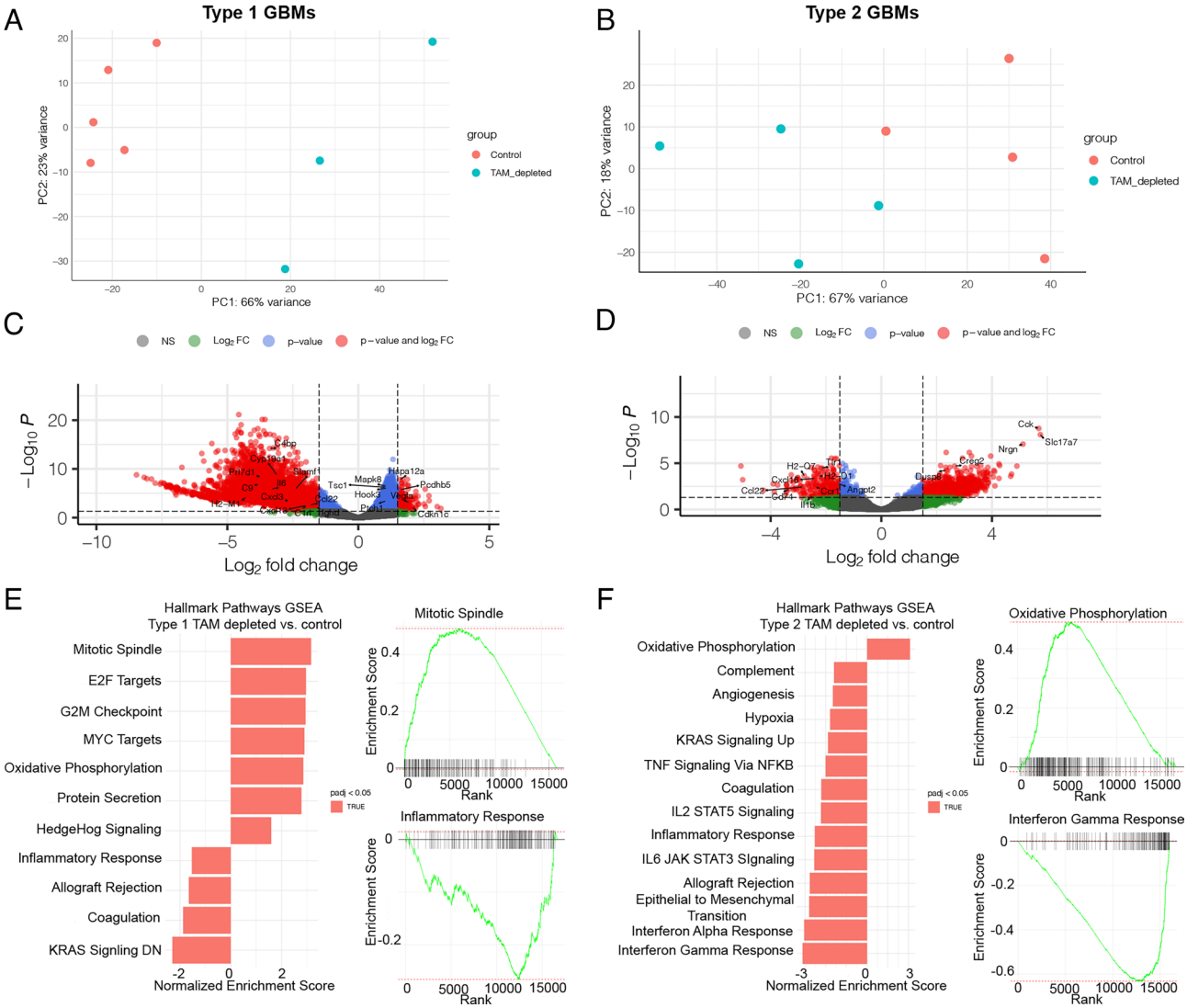

Fig. 4. Type 1 and Type 2 GBMs have distinct molecular responses to TAM depletion. (*A*) PCA plot showing Type 1 TAM-depleted vs. control samples. (*B*) PCA plot showing Type 2 TAM-depleted vs. control samples. (*C*) Volcano plot showing the DEGs when comparing Type 1 TAM-depleted vs. all control tumors (padj < 0.05, LFC > 1.5 or <−1.5). (*D*) Volcano plot showing the DEGs when comparing Type 2 TAM-depleted vs. all control tumors (padj < 0.05, LFC > 1.5 or <−1.5). (*E*) Hallmark pathway GSEA of Type 1 TAM-depleted vs. control tumors. Select enrichment plots for mitotic spindle and inflammatory response shown. (*F*) Hallmark pathway GSEA of Type 2 TAM-depleted vs. control tumors. Select enrichment plots for oxidative phosphorylation and interferon gamma response shown.

that TAM transcriptional differences were driven primarily by ontogeny and not by model type. Thus, the orthotopic transplantation models can be considered physiologically relevant models for TAM studies.

A central question addressed in this study was to evaluate the extent of TAM contribution to tumor development and progression as previous GBM mouse model studies have reported contrasting results and employed models of varying relatedness to stereotypic mutations found in GBM (9, 14, 17, 30). We initiated studies for in vivo TAM depletion using two previously described methods: diphtheria toxin-mediated ablation (29, 36) and CSF1R receptor inhibition (14). We found that either method alone had limitations. Diphtheria toxin receptor expression, activated by Cre-mediated recombination of the silenced floxed allele in TAMs results in rapid depletion to >85% levels by 24 h. However, within 72 h, we observed robust TAM repopulation by microglia that were not expressing the CX3CR1-driven Cre recombinase iDTR transgene. The result was complete repopulation of a DT-resistant microglial population within 1 wk and thus only provided transitory TAM depletion. The alternative approach of CSF1R inhibition provided different outcomes. Constant exposure to the CSF1R inhibitor in the mouse chow afforded more effective chronic TAM reduction but took one week to reach maximal depletion levels of ~80%. We therefore adopted a combined protocol in which mice were fed CSF1R inhibitor chow after exposure to DT. This combined approach allowed us to achieve immediate and sustained TAM depletion to around 85 to 95% over the course of our experiments.

Robust TAM depletion did not extend survival or impact tumor cell proliferation and histology in either Type 1 or Type 2 GBMs. To understand the molecular impact of TAM depletion, we performed bulk RNA-sequencing on Type 1 and Type 2 TAM-depleted and control GBMs. We found that despite TAM depletion, Type 1 and Type 2 GBMs retained their lineage-associated transcriptomes. However, when we analyzed Type 1 and Type 2 samples independently, we found that they had differing transcriptomic responses to TAM depletion therapy; Type 1 TAM-depleted GBMs had greater expression of progrowth pathways than Type 2 TAM-depleted GBMs. Additionally, Type 2 TAM-depleted GBMs had diminished expression of more immune-related hallmark

pathways than Type 1 GBM, consistent with the greater immune component of Type 2 GBMs. Thus, we show that although Type 1 and Type 2 GBM can both progress in the absence of TAMs, their molecular response to TAM depletion differs.

As our tumor models have an *Nf1* deletion, this adds to previous observations made in an H-Ras–driven model of GBM that Ras-driven GBMs are inherently nonresponsive to TAM depletion (17). Here, we also performed TAM depletion in a GBM model system that lacks an *Nf1* mutation (*Nst-CreER^{T2}; Qk$^{fl/fl}$; Trp53$^{fl/fl}$; Pten$^{fl/fl}$*) (31), and tumors progressed equivalently in the absence of TAMs. Taken together, these results suggest that possibly only a specific subset of GBM models, such as PDGFB-driven GBMs (14), require TAMs for optimal tumor progression. Thus far, there have been no statistically significant correlations found between tumor genetics and responses to CSF1R therapy in clinical trials (16). One patient in the trial showing extended PFS had an *Nf1* alteration, but the limited trial size was insufficient to provide statistical power (16). A larger trial will be needed to determine if there are any statistically significant correlations with GBM genetic alterations. Alternatively, there may exist intrinsic biological features of different model systems that add complexity to the tumor immune microenvironment and continued vigilance to adhere to physiologically relevant model systems will be an ever-increasing priority. Taken together, these studies highlight the heterogeneity of TAMs and response to CSF1R inhibitor across GBM mouse model systems.

Our results put into question the relevance of therapies aimed at ablating TAMs in the GBM tumor immune microenvironment and indicate a possible explanation for the failure of TAM depletion therapy in clinical trials. However, potentially impactful insights come from the observation that Type 2 tumors have a particularly high level of MDM infiltration. This suggests the possibility that therapeutics harnessing MDMs may have a unique and selective therapeutic efficacy on patients harboring Type II GBM.

Methods

Mice. All mouse experiments were approved and performed according to the guidelines of the Institutional Animal Care and Use Committee of Memorial Sloan Kettering Cancer Center. Tumor suppressor mice with Nestin-CreER^{T2} (37–39) or NG2-CreER^{TM} (19, 40) transgenes were crossed with conditional *Trp53* allele. Nestin-CreER^{T2}; *Nf1*$^{fl/+}$; *Trp53*$^{fl/fl}$; *Pten*$^{fl/+}$ mice or NG2-CreER^{TM}; *Nf1*$^{fl/+}$; *Trp53*$^{fl/fl}$; *Pten*$^{fl/+}$ mice were generated by breeding Nestin-CreER^{T2};*Trp53*$^{fl/fl}$ or NG2-CreER^{TM};*Trp53*$^{fl/fl}$ mice with *Nf1*$^{fl/fl}$; *Trp53*$^{fl/fl}$; *Pten*$^{fl/fl}$ mice. All mice were maintained under formal MSKCC IACUC protocols.

Cx3cr1-CreER^{T2}-Ires-Eyfp mice (29) (JAX Stock #: 021160) were bred to *Rosa26-Lsl-Tdt* mice (JAX Stock#: 007908). These mice were then bred to *Rosa26-Lsl-iDTR* mice (41) (JAX Stock#: 007900) *to get Cx3cr1-CreER^{T2}-Ires-Eyfp; Rosa26-Lsl-Tdt/iDTR* mice.

Mouse Primary Cell Culture. Mice with tumor suppressor alleles were induced with tamoxifen at 4 to 6 wk of age and aged until they developed symptoms of GBM as described previously (18). Symptomatic mice were anesthetized and transcardially perfused with ice-cold HBSS and tissues were harvested. The tissues were chopped and incubated with Accutase in a 37 °C water bath for 20 min, dissociated, and cultured in a serum-free medium supplemented with B27 and N2 (serum-free media), plus EGF, FGF, and PDGF-AA (10 ng/mL each) for Type 1 GBMs (both *Nf1*$^{-/-}$ and *Nf1* WT), and EGF, FGF, and Neuregulin (10 ng/mL each) for Type 2 GBM. Cells were kept in 5% oxygen, 37 °C incubator. Primary cultures were established as tumor spheres at P0, later passages were as spheres in non-coated plates, or as monolayer in laminin-precoated plates (10 ng/mL Laminin diluted in DPBS with Ca2+/Mg2+).

Mouse Stereotactic GBM Cell Injection. The Type 1 and Type 2 GBM cell lines were derived from spontaneous GBM mice and cultured as described above. For intracranial injection, mice were anesthetized (Isoflurane) and placed on a stereotactic frame. A midline incision was made on the skin to expose the skull, and a microdrill was used to perform craniotomy. For intracranial injection, 1×10^4 cells were injected in the striatum (coordinates: 1.0 AP, −1.8 ML, 4.5 DV with respect to the bregma). Minimum cells were injected to avoid inducing inflammation and to model physiologic conditions as closely as possible. Mice were monitored and killed for tissue collection when neurologic symptoms were evident.

Tumor Dissociation. Mice were anesthetized and transcardially perfused with ice-cold HBSS. Tumors were dissected, chopped up on ice, and dissociated using the Miltenyi Brain Tumor Dissociation Kit. Following dissociation, the myelin was removed with the Miltenyi myelin removal beads and magnetic separator. Next, red blood cells were removed with red blood cell lysis buffer (Sigma). Tumor cell suspensions were frozen with BamBanker cell freezing media and placed at −80 for <1 mo prior to flow cytometry studies.

Histology and Immunohistochemistry. Mice were perfused with PBS and brains were fixed in 4% paraformaldehyde, processed, and embedded into paraffin blocks. Blocks were sectioned into 10 μM sections and stored at four degrees until staining. DAPI was used to stain the nucleus (ThermoScientific, 1 μg/mL). All immunofluorescent antibodies used are listed in *SI Appendix*, Table S1. The sections were then imaged with a Zeiss LSM 510 confocal microscope using Argon 488, He543, and He 633. Images were quantified using Fiji.

Multicolor Flow Cytometry. Tumor cell suspensions were dethawed and stained with a fixable viability dye. Cells were then washed, blocked with CD16/32 Fc block for 5 to 10 min, and stained with extracellular antibodies for 20 min on ice. Cells were then washed and either resuspended in FACS buffer or FluoroFix buffer (BioLegend) for analysis (myeloid panel) or moved on for staining with intracellular antibody FoxP3 (lymphoid panel). For intracellular staining, cells were fixed and permeabilized with the FoxP3/transcription factor staining kit (eBioscience). Then, cells were stained with FoxP3 for 30 min on ice, washed, and resuspended in FACS buffer for analysis. Flow cytometry data were acquired using BD Biosciences LSRFortessa analyzers and BD FACSDiva software. Data were analyzed using FlowJo. All flow cytometry antibodies are listed in *SI Appendix*, Table S2.

TAM Depletion. *Cx3cr1-CreER^{T2}-Ires-Eyfp; Rosa26-Lsl-Tdt/iDTR* mice were induced with tamoxifen (10 mg/20 g body weight) with oral gavage at 4 to 6 wk of age twice, 24 h apart. Then, 1 to 2 wk following tamoxifen induction, mice were stereotactically injected with 1×10^4 Type 1 or Type 2 GBM cells. Mice were monitored by bioluminescence imaging or MRI for tumor formation. Approximately 3 to 4 wk following stereotactic injection, mice were treated with DT (50 ng/20 g body weight) or DPBS for the control group, three times, 24 h apart. Following the last dose of diphtheria toxin, mice were placed on PLX5622 CSF1R inhibitor chow (Plexxicon) or control chow for the remainder of their life. PLX5622 was incorporated into AIN-76A Rodent Diet at a 1,200 mg/kg concentration by Research Diets. Mice were monitored until neurologic symptoms emerged and then were killed for tissue collection. Survival curves were made using a prism, and the log-rank Mantel–Cox test was used to test for significance. Data are representative of several independent experiments. TAM depletion in normal brains was estimated by comparing the median values for the cortex region. For tumor-bearing brains, TAM depletion percentage was estimated by comparing the percentages of total TAMs between TAM-depleted and control Type 1 and Type 2 tumors.

Analysis of TCGA GBM Data. Gene expression data from TCGA samples previously subtyped as core Type 1 or Type 2 (18) GBMs was used to look at the relative levels of immune marker genes. Significance was calculated using a Wilcox test with the R package ggsignif.

Bulk RNA-Sequencing.

RNA extraction.

Sorted TAM RNAseq (related to SI Appendix, Fig. S3). Following tumor dissection, tumors were stained with CD45, Ly6C, Ly6G, and CD11B (*SI Appendix*, Table S2) and sorted for Microglia (Ly6C$^-$, Ly6G$^-$, CD45^{lo}, CD11B$^+$) and MDMs (Ly6C$^-$, Ly6G$^-$, CD45^{hi}, CD11B$^+$) directly into Trizol LS and flash-frozen at −80. RNA was then extracted by the standard Trizol LS protocol.

Bulk tumor tissue RNAseq (related to Fig. 4). At tumor dissection, a small tumor piece was flash-frozen and stored at −80. Later, tumor pieces were lysed in Trizol and RNA was extracted using the Zymo Direct-zol RNA Mini Prep Kit (R2050). Samples were eluted in 20 μL RNase-free water and submitted for RNAseq.

Transcriptome sequencing.

Sorted TAM RNAseq (related to SI Appendix, Fig. S3). After RiboGreen quantification and quality control by Agilent BioAnalyzer, 1.1 to 2.0 ng total RNA with RNA integrity numbers ranging from 7.2 to 10 underwent amplification using the SMART-Seq v4 Ultra Low Input RNA Kit (Clonetech catalog # 63488), with 12 cycles of amplification. Next, 1 to 4 ng of amplified cDNA was used to prepare libraries with the KAPA Hyper Prep Kit (Kapa Biosystems KK8504) using eight cycles of PCR. Samples were barcoded and run on a NovaSeq 6000 in a PE50 run, using the NovaSeq 6000 S1 Reagent Kit (100 Cycles) (Illumina). An average of 59 million paired reads were generated per sample, and the percent of mRNA bases per sample ranged from 77 to 88%.

Bulk tumor tissue RNAseq (related to Fig. 4). This was performed by Admera Health sequencing services. Isolated RNA sample quality was assessed by RNA ScreenTape on a Tapestation (Agilent Technologies Inc. and quantified by Qubit 2.0 RNA HS assay (Thermo Fisher). Ribosomal RNA depletion was performed with QIAseq® FastSelect rRNA HMR kit (Qiagen) as per the manufacturer's instructions. All library constructions were prepared according to the NEBNext® UltraTM II Directional RNA Library Prep Kit for Illumina® (New England BioLabs Inc.). Final libraries quantity was assessed by Qubit 2.0 (Thermo Fisher) and quality was assessed by TapeStation HSD1000 ScreenTape (Agilent Technologies Inc.). The final library size was about 450 bp with an insert size of about 300 bp. Illumina® 8-nt dual-indices were used. Equimolar pooling of libraries was performed based on QC values and sequenced on an Illumina® Novaseq S4 (Illumina) with a read length configuration of 150 PE for 60 M PE reads per sample (30 M in each direction).

Downstream Analysis of Bulk RNAseq Data.

Alignment. Samples were aligned using STAR to the mouse GRCm39 or GRCm38 reference genome for the sorted TAM RNAseq and the TAM depletion tumor RNAseq, respectively.

DEG analysis. DESeq2 (42) was used for differential gene expression analysis for all bulk RNAseq studies. DEGs were reported that had a padj < 0.05, and LFC > 1.5 or <−1.5. Volcano plots were made using the EnhancedVolcano package.

GO analysis. GO was performed using the lists of significantly increased or decreased DEGs with the ClusterProfiler, TopGO, and DOSE packages.

GSEA analysis. GSEA analysis was performed using the gene level statistic values found in the DESeq2 differential expression results file as a ranking metric. The R package fgsea was used for this analysis.

Statistical Analysis. Statistical analysis between groups was performed using two-tailed unpaired Student's *t* test unless otherwise indicated. Kaplan–Meier survival curves were analyzed using log-rank (Mantel Cox) test. Data were analyzed using GraphPad Prism v.9 and Fiji. *P* values less than 0.05 were considered significant unless otherwise indicated.

Data, Materials, and Software Availability. RNAseq data have been deposited in Gene expression omnibus under accession numbers GSE225827 (43), GSE226050 (44), and GSE226051 (45).

ACKNOWLEDGMENTS. We would like to thank members of the Parada Lab for helpful suggestions and discussion. We acknowledge the use of the Integrated Genomics Operation Core, funded by the NCI Cancer Center Support Grant (CCSG, P30 CA08748), Cycle for Survival, and the Marie-Josée and Henry R. Kravis Center for Molecular Oncology. We acknowledge the Flow Cytometry Core Facility, partially funded by NCI/NIH Cancer Center Grant (P30: CA008748), and Kathleen Daniels specifically for assistance in designing the multicolor flow cytometry panels used in this study. We acknowledge the Jian Hu lab for providing us with the GBM primary culture line from spontaneous mouse GBM derived from *Nst-CreER^{T2}; Qk$^{fl/fl}$; Trp53$^{fl/fl}$; Pten$^{fl/fl}$* mice for this study. We acknowledge Plexxicon for providing PLX5622 for these studies. M.E.C. was funded by an NCI NRSA F31 Predoctoral Fellowship (F31:CA247463). L.F.P. received funding from the NCI (NCI R35:CA210100, R01:CA131313, SPORE: U54 CA196519-01) and in part from the NIH/NCI Cancer Center Support Grant (P30: CA008748). L.F.P. holds the Albert C. Foster Chair in cancer research. L.F.P. also acknowledges the support of the Ivy Foundation, Cancer Research UK, and the MSKCC Ludwig Center for Immunotherapy Research.

Author affiliations: [a]Brain Tumor Center, Memorial Sloan Kettering Cancer Center, New York, NY 10065; [b]Cancer Biology & Genetics Program, Memorial Sloan Kettering Cancer Center, New York, NY 10065; [c]Louis V. Gerstner, Jr. Graduate School of Biomedical Sciences, Memorial Sloan Kettering Cancer Center, New York, NY 10065; and [d]Department of Pathology, Memorial Sloan Kettering Cancer Center, New York, NY 10065

Author contributions: M.E.C., Z.W., D.S., and L.F.P. designed research; M.E.C., Z.W., D.S., and A.M.P. performed research; M.E.C. contributed new reagents/analytic tools; M.E.C., T.A.B., and L.F.P. analyzed data; and M.E.C. and L.F.P. wrote the paper.

1. Q. T. Ostrom *et al.*, CBTRUS Statistical report: primary brain and other central nervous system tumors diagnosed in the United states in 2009–2013. *Neuro Oncol.* **18**, v1–v75 (2016).
2. R. Stupp *et al.*, Effect of tumor-treating fields plus maintenance temozolomide vs maintenance temozolomide alone on survival in patients with glioblastoma: A randomized clinical trial. *JAMA* **318**, 2306–2316 (2017).
3. F. Klemm *et al.*, Interrogation of the microenvironmental landscape in brain tumors reveals disease-specific alterations of immune cells. *Cell* **181**, 1643–1660.e1617 (2020).
4. D. Hambardzumyan, D. H. Gutmann, H. Kettenmann, The role of microglia and macrophages in glioma maintenance and progression. *Nat. Neurosci.* **19**, 20–27 (2016).
5. H. Liu *et al.*, Pro-inflammatory and proliferative microglia drive progression of glioblastoma. *Cell Rep.* **36**, 109718 (2021).
6. C. Zhu, J. M. Kros, C. Cheng, D. Mustafa, The contribution of tumor-associated macrophages in glioma neo-angiogenesis and implications for anti-angiogenic strategies. *Neuro Oncol.* **19**, 1435–1446 (2017).
7. Y. Shi *et al.*, Tumour-associated macrophages secrete pleiotrophin to promote PTPRZ1 signalling in glioblastoma stem cells for tumour growth. *Nat. Commun.* **8**, 15080 (2017).
8. P. Chen *et al.*, Symbiotic macrophage-glioma cell interactions reveal synthetic lethality in PTEN-Null glioma. *Cancer Cell* **35**, 868–884.e866 (2019).
9. A. R. Pombo Antunes *et al.*, Single-cell profiling of myeloid cells in glioblastoma across species and disease stage reveals macrophage competition and specialization. *Nat. Neurosci.* **24**, 595–610 (2021).
10. N. Ochocka *et al.*, Single-cell RNA sequencing reveals functional heterogeneity of glioma-associated brain macrophages. *Nat. Commun.* **12**, 1151 (2021).
11. A. T. Yeo *et al.*, Single-cell RNA sequencing reveals evolution of immune landscape during glioblastoma progression. *Nat. Immunol.* **23**, 971–984 (2022), 10.1038/s41590-022-01215-0.
12. H. J. Kim *et al.*, Blood monocyte-derived CD169(+) macrophages contribute to antitumor immunity against glioblastoma. *Nat. Commun.* **13**, 6211 (2022).
13. A. Christofides *et al.*, The complex role of tumor-infiltrating macrophages. *Nat. Immunol.* **23**, 1148–1156 (2022).
14. S. M. Pyonteck *et al.*, CSF-1R inhibition alters macrophage polarization and blocks glioma progression. *Nat. Med.* **19**, 1264–1272 (2013).
15. D. F. Quail *et al.*, The tumor microenvironment underlies acquired resistance to CSF-1R inhibition in gliomas. *Science* **352**, aad3018 (2016).
16. N. Butowski *et al.*, Orally administered colony stimulating factor 1 receptor inhibitor PLX3397 in recurrent glioblastoma: An ivy foundation early phase clinical trials consortium phase II study. *Neuro Oncol.* **18**, 557–564 (2016).
17. R. Rao *et al.*, Glioblastoma genetic drivers dictate the function of tumor-associated macrophages/microglia and responses to CSF1R inhibition. *Neuro Oncol.* **24**, 584–597 (2022).
18. Z. Wang *et al.*, Cell lineage-based stratification for glioblastoma. *Cancer Cell* **38**, 366–379.e368 (2020).
19. S. R. Alcantara Llaguno *et al.*, Adult lineage-restricted CNS progenitors specify distinct glioblastoma subtypes. *Cancer Cell* **28**, 429–440 (2015).
20. Z. Chen, J. L. Ross, D. Hambardzumyan, Intravital 2-photon imaging reveals distinct morphology and infiltrative properties of glioblastoma-associated macrophages. *Proc. Natl. Acad. Sci. U.S.A.* **116**, 14254–14259 (2019).
21. R. L. Bowman *et al.*, Macrophage ontogeny underlies differences in tumor-specific education in brain malignancies. *Cell Rep.* **17**, 2445–2459 (2016).
22. D. B. Zamler *et al.*, Immune landscape of a genetically engineered murine model of glioma compared with human glioma. *JCI Insight* **7**, e148990 (2022).
23. R. G. Verhaak *et al.*, Integrated genomic analysis identifies clinically relevant subtypes of glioblastoma characterized by abnormalities in PDGFRA, IDH1, EGFR, and NF1. *Cancer Cell* **17**, 98–110 (2010).
24. C. W. Brennan *et al.*, The somatic genomic landscape of glioblastoma. *Cell* **155**, 462–477 (2013).
25. A. Buttgereit *et al.*, Sall1 is a transcriptional regulator defining microglia identity and function. *Nat. Immunol.* **17**, 1397–1406 (2016).
26. T. R. Hammond *et al.*, Single-Cell RNA sequencing of microglia throughout the mouse lifespan and in the injured brain reveals complex cell-state changes. *Immunity* **50**, 253–271.e256 (2019).
27. M. L. Bennett *et al.*, New tools for studying microglia in the mouse and human CNS. *Proc. Natl. Acad. Sci. U.S.A.* **113**, E1738–1746 (2016).
28. Z. Chen *et al.*, Cellular and molecular identity of tumor-associated macrophages in glioblastoma. *Cancer Res.* **77**, 2266–2278 (2017).
29. C. N. Parkhurst *et al.*, Microglia promote learning-dependent synapse formation through brain-derived neurotrophic factor. *Cell* **155**, 1596–1609 (2013).

30. H. Galarneau, J. Villeneuve, G. Gowing, J. P. Julien, L. Vallieres, Increased glioma growth in mice depleted of macrophages. *Cancer Res.* **67**, 8874–8881 (2007).
31. T. Shingu *et al.*, Qki deficiency maintains stemness of glioma stem cells in suboptimal environment by downregulating endolysosomal degradation. *Nat. Genet* **49**, 75–86 (2017).
32. A. Mantovani, P. Allavena, F. Marchesi, C. Garlanda, Macrophages as tools and targets in cancer therapy. *Nat. Rev. Drug Discov.* **21**, 799–820 (2022).
33. C. A. von Roemeling *et al.*, Therapeutic modulation of phagocytosis in glioblastoma can activate both innate and adaptive antitumour immunity. *Nat. Commun.* **11**, 1508 (2020).
34. N. Jiang *et al.*, Fatty acid oxidation fuels glioblastoma radioresistance with CD47-mediated immune evasion. *Nat. Commun.* **13**, 1511 (2022).
35. M. De Palma *et al.*, Tumor-targeted interferon-alpha delivery by Tie2-expressing monocytes inhibits tumor growth and metastasis. *Cancer Cell* **14**, 299–311 (2008).
36. J. Bruttger *et al.*, Genetic cell ablation reveals clusters of local self-renewing microglia in the mammalian central nervous system. *Immunity* **43**, 92–106 (2015).
37. S. Alcantara Llaguno *et al.*, Malignant astrocytomas originate from neural stem/progenitor cells in a somatic tumor suppressor mouse model. *Cancer Cell* **15**, 45–56 (2009).
38. J. Chen, C. H. Kwon, L. Lin, Y. Li, L. F. Parada, Inducible site-specific recombination in neural stem/progenitor cells. *Genesis* **47**, 122–131 (2009).
39. M. Groszer *et al.*, Negative regulation of neural stem/progenitor cell proliferation by the Pten tumor suppressor gene in vivo. *Science* **294**, 2186–2189 (2001).
40. X. Zhu *et al.*, Age-dependent fate and lineage restriction of single NG2 cells. *Development* **138**, 745–753 (2011).
41. T. Buch *et al.*, A Cre-inducible diphtheria toxin receptor mediates cell lineage ablation after toxin administration. *Nat. Methods* **2**, 419–426 (2005).
42. M. I. Love, W. Huber, S. Anders, Moderated estimation of fold change and dispersion for RNA-seq data with DESeq2. *Genome Biol.* **15**, 550 (2014).
43. M. E. Chipman, L. F. Parada, Tumor progression is independent of tumor associated macrophages in two lineage-based mouse models of GBM [SortedTAM RNAseq]. *GEO*. https://www.ncbi.nlm.nih.gov/geo/query/acc.cgi?acc=GSE225827. Deposited 6 March 2023.
44. M. E. Chipman, L. F. Parada, Tumor progression is independent of tumor associated macrophages in two lineage-based mouse models of GBM[TAMdepletedVsControl RNAseq]. *GEO*. https://www.ncbi.nlm.nih.gov/geo/query/acc.cgi?acc=GSE226050. Deposited 6 March 2023
45. M. E. Chipman, L. F. Parada, Tumor progression is independent of tumor associated macrophages in two lineage-based mouse models of GBM SuperSeries. *GEO*. https://www.ncbi.nlm.nih.gov/geo/query/acc.cgi?acc=GSE226051. Deposited 6 March 2023.